Unconditionally Stable Divergence-Free Vector Meshless Method Based on Crank–Nicolson Scheme

Sheyda Shams and Masoud Movahhedi, *Member, IEEE*

***Abstract*—This letter presents the Crank–Nicolson formulation of vector meshless method. As the vector meshless method is divergence-free, its solutions are more precise than the conventional scalar meshless methods. In the conventional time-domain vector meshless method, the time-step size is restricted by Courant–Friedrichs–Lewy criterion. In order to attain an unconditionally stable formulation of vector meshless method, we have applied the Crank–Nicolson scheme to this method. Moreover, by a numerical example, we have investigated the efficiency and accuracy of the proposed method in comparison to another unconditionally stable vector meshless method, i.e., alternating-direction-implicit vector meshless method.**

***Index Terms*—Alternating-direction-implicit (ADI) method, Crank–Nicolson (CN) scheme, divergence-free property, unconditionally stable, vector meshless method.**

I. Introduction

MESHLESS methods were first proposed about two decades ago. For years, these methods have been acknowledged as the robust numerical methods among classical time-domain numerical techniques. In meshless methods, the discretization scheme of spatial domain alters from grid/cell-based numerical methods, and the problem domains are discretized through spatial nodes rather than grid/cells. Moreover, as no information on the connectivity manner of the spatial nodes is required in these methods, simulation of complicated structures do not have the difficulties of the conventional numerical methods.

Up to now, a vast range of the meshless methods has been developed. The radial basis function (RBF) method is one of the most powerful meshless methods, which was proposed by Lai *et al.* [1], for analyzing time-domain electromagnetic problems. The RBF meshless method due to the scalar form of its RBFs is an efficient tool for solving the scalar form of the differential formulation of Maxwell's equations. On the other hand, Yang *et al.* [2] have proposed vector meshless method that is formulated based on the vector RBFs. These RBFs are defined by applying a matrix transform to the scalar RBFs. The obtained vector RBFs result in vector shape functions and provide a facility for expanding the vector fields of Maxwell's equations.

Manuscript received June 10, 2017; revised July 14, 2017; accepted August 9, 2017. Date of publication August 17, 2017; date of current version September 25, 2017. *(Corresponding Author: Masoud Movahhedi.)*

The authors are with the Department of Electrical Engineering, Yazd University, Yazd 89195-741, Iran (e-mail: sh.shams@stu.yazd.ac.ir; sh.shams70@gmail.com; movahhedi@yazd.ac.ir).

Color versions of one or more of the figures in this letter are available online at http://ieeexplore.ieee.org.

Digital Object Identifier 10.1109/LAWP.2017.2740379

Vector meshless method is of considerable significance since its solutions are divergence-free. This property is due to the divergence-free property of the vector RBFs and improves the accuracy of vector meshless method compared to the scalar RBF meshless methods. However, as the time-marching formulation of the conventional vector meshless method is based on the explicit form, the maximum time-step size is restricted by Courant-Friedrichs-Lewy criterion.

To overcome the conditional stability of the numerical methods, some well-known algorithms have been proposed in various studies. The Crank–Nicolson (CN) scheme is one of the efficient algorithms that is used for achieving the unconditionally stable formulation of the finite-difference time domain (FDTD) methods [3], [4], finite element method [5], and conventional scalar meshless method [6]. Another scheme that can lead to unconditionally stable property is alternating-direction-implicit (ADI) algorithm. Applications of this scheme in meshless methods have been investigated for the scalar meshless method in [7] and [8] and for vector meshless method in [9] and [10].

Incorporating the CN scheme into a scalar meshless method [6] or FDTD method [11] leads to a smaller numerical velocity anisotropy error compared to the ADI scheme. In addition, Zhu *et al.* [6] have showed that the computational efficiency of the conventional scalar meshless method based on the CN scheme is higher than its ADI counterpart. Therefore, in this letter, we have incorporated the CN scheme into vector meshless method. The CN formulation of vector meshless method has two important properties of the unconditional stability and being divergence-preserved.

II. CN Formulation of Vector Meshless Method

A. Formulation of Vector Basis Functions and Vector Shape Functions

As vector meshless method is formulated based on the divergence-free vector RBFs, its formulation is alternative from the conventional scalar RBF method in [12]. Therefore, first we briefly explain the formulation of vector meshless method. Yang *et al.* [2] have presented the complete details of the formulation of vector meshless method, which is based on the proposed vector RBFs in [13]–[15].

In order to analyze a problem with meshless method, its spatial domain and boundary is represented by N nodes. An unknown function value at a point of interest can be approximated by interpolating the function values at the surrounding nodes of the point of interest. To interpolate an unknown divergence-free vector field, denoted as $\boldsymbol{u}$, first we should obtain the vector RBFs. The vector RBFs can be constructed from a (3×3) matrix transform, which should be applied to a scalar RBF [2]. In this letter, we have chosen the Gaussian function as the scalar

RBF. The following equation shows the scalar RBFϕ_j related to node *j* as [2]:

$$\phi_j = \phi\left(\|\mathbf{x}-\mathbf{x}_j\|\right) = e^{-\alpha\left[(x-x_j)^2+(y-y_j)^2+(z-z_j)^2\right]} \tag{1}$$

where $\mathbf{x}=(x,y,z)$ is the location of the point of interest, $\mathbf{x}_j=(x_j,y_j,z_j)$ is the location of node *j* surrounding the point of interest, $\|\mathbf{x}-\mathbf{x}_j\|$ is the Euclidean distance between the point of interest and the node *j*, and α is the shape parameter that affects the performance of the Gaussian function.

The mentioned matrix transform that leads to divergence-free vector RBFs $\mathbf{\Psi}_j$ related to each node and the vector shape function $\mathbf{\Phi}$ can be expressed as [2]

$$\mathbf{\Psi}_j = (-\Delta\mathbf{I}+\nabla\nabla^T)\phi_j \tag{2}$$

$$\mathbf{\Phi} = \mathbf{B}_v\mathbf{A}_v{}^{-1}\mathbf{u}_s \tag{3}$$

where Δ is the (3×3) Laplace operator of Cartesian coordinate system, $\mathbf{I}$ is a (3×3) identity matrix, ϕ_j is the scalar RBF related to node *j*, $\nabla^T=[\partial/\partial x,\partial/\partial y,\partial/\partial z]$, $\nabla=[\partial/\partial x,\partial/\partial y,\partial/\partial z]^T$, $\mathbf{u}_s=[\ldots\ u_{jx}\ u_{jy}\ u_{jz}\ \ldots]^T$, $\mathbf{B}_v$ includes vector RBFs, and

$$\mathbf{A}_v = \begin{bmatrix} \mathbf{\Psi}(\|\mathbf{x}_1-\mathbf{x}_1\|) & \mathbf{\Psi}(\|\mathbf{x}_1-\mathbf{x}_2\|) & \ldots & \mathbf{\Psi}(\|\mathbf{x}_1-\mathbf{x}_N\|) \\ \mathbf{\Psi}(\|\mathbf{x}_2-\mathbf{x}_2\|) & \mathbf{\Psi}(\|\mathbf{x}_2-\mathbf{x}_2\|) & \ldots & \mathbf{\Psi}(\|\mathbf{x}_2-\mathbf{x}_N\|) \\ \vdots & \vdots & & \vdots \\ \mathbf{\Psi}(\|\mathbf{x}_N-\mathbf{x}_1\|) & \mathbf{\Psi}(\|\mathbf{x}_N-\mathbf{x}_2\|) & \ldots & \mathbf{\Psi}(\|\mathbf{x}_N-\mathbf{x}_N\|) \end{bmatrix}_{3N\times 3N} \tag{4}$$

Then, the approximation of the unknown vector field ***u*** based on the vector shape function related to each node *j*, i.e., $\mathbf{\Phi}_j$, can be expressed as

$$\mathbf{u} = \sum_{j=1}^{N} \mathbf{\Phi}_j\mathbf{u}_j \tag{5}$$

where $\mathbf{u}_j=[u_{jx}\ u_{jy}\ u_{jz}]^T$.

Similarly, we can approximate the electric and magnetic vector fields by the vector shape function $\mathbf{\Phi}_j$ related to node *j* as

$$\mathbf{E} = \sum_{j}^{NE} \mathbf{\Phi}_j\mathbf{E}_j \tag{6a}$$

$$\mathbf{H} = \sum_{j}^{NH} \mathbf{\Phi}_j\mathbf{H}_j \tag{6b}$$

where $\mathbf{E}_j=[E_{jx}\ E_{jy}\ E_{jz}]^T$ and $\mathbf{H}_j=[H_{jx}\ H_{jy}\ H_{jz}]^T$.

B. Applying the CN Scheme to Vector Meshless Method

As in vector meshless method the electromagnetic fields are in their vector forms, the process of incorporating the CN scheme into vector meshless method is different from that which has been done for the scalar RBF meshless method.

In order to derive our formulation, first we consider the differential form of Maxwell's equations without current sources in Cartesian coordinate system. In the CN scheme, for finding the spatial derivative of each component of the electromagnetic field with respect to *x, y,* or *z* in $(n+1/2)$th time-step, we approximate the spatial derivative through the average of the spatial derivative in the $(n+1)$th and (n)th time-steps. On the other hand, we use the central difference approximation to calculate the time derivatives [6]. Based on this procedure, the following equations are obtained:

$$E_x{}^{n+1} = E_x{}^{n} + \frac{\Delta t}{2\varepsilon}\left(\frac{\partial H_z{}^{n+1}}{\partial y}+\frac{\partial H_z{}^{n}}{\partial y}-\frac{\partial H_y{}^{n+1}}{\partial z}-\frac{\partial H_y{}^{n}}{\partial z}\right) \tag{7}$$

$$H_x{}^{n+1} = H_x{}^{n} + \frac{\Delta t}{2\mu}\left(\frac{\partial E_y{}^{n+1}}{\partial z}+\frac{\partial E_y{}^{n}}{\partial z}-\frac{\partial E_z{}^{n+1}}{\partial y}-\frac{\partial E_z{}^{n}}{\partial y}\right) \tag{8}$$

By cyclic permutations of subscripts x,y,z in (7) and (8), we obtain the other components of the electric and magnetic fields, respectively. Then, we consider (7) and substitute the $(n+1)$th time-step of the magnetic field components into (7). Similarly, by considering the other components of the electric field and substituting the $(n+1)$th time-step of the magnetic field components into them, we obtain the implicit equations for the electric field. One of the components of the electric field is shown in (9) at the bottom of the page and the other components can be obtained with cyclic permutations.

As in vector meshless method, the vector form of the Maxwell curl equations is considered, we collect (9) and its cyclic permutations to obtain the electric field in its vector form. The following equation shows the obtained implicit formulation for the vector of electric field based on the CN scheme:

$$\mathbf{E}^{n+1} + \frac{\Delta t^2}{4\mu\varepsilon}\nabla\times\left(\nabla\times\mathbf{E}^{n+1}\right) = \mathbf{E}^{n} + \frac{\Delta t}{\varepsilon}\nabla\times\mathbf{H}^{n} - \frac{\Delta t^2}{4\mu\varepsilon}\nabla\times\left(\nabla\times\mathbf{E}^{n}\right). \tag{10}$$

Then, according to (6a) and (6b), we use the vector shape functions of the electric and magnetic fields to approximate the spatial derivatives in (10). Finally, due to the Kronecker's delta property of the vector shape function, the vector of the electric

$$E_x{}^{n+1}\hat{a}_x + \frac{\Delta t^2}{4\mu\varepsilon}\left(\frac{\partial^2 E_y{}^{n+1}}{\partial y\partial x}-\frac{\partial^2 E_x{}^{n+1}}{\partial y^2}+\frac{\partial^2 E_z{}^{n+1}}{\partial z\partial x}-\frac{\partial^2 E_x{}^{n+1}}{\partial z^2}\right)\hat{a}_x = E_x{}^{n}\hat{a}_x + \frac{\Delta t}{\varepsilon}\left(\frac{\partial H_z{}^{n}}{\partial y}-\frac{\partial H_y{}^{n}}{\partial z}\right)\hat{a}_x + \frac{\Delta t^2}{4\mu\varepsilon}\left(\frac{\partial^2 E_x{}^{n}}{\partial y^2}-\frac{\partial^2 E_y{}^{n}}{\partial y\partial x}-\frac{\partial^2 E_z{}^{n}}{\partial z\partial x}+\frac{\partial^2 E_x{}^{n}}{\partial z^2}\right)\hat{a}_x \tag{9}$$

field can be updated implicitly as

$$\mathbf{E}_i^{n+1} + \frac{\Delta t^2}{4\mu\varepsilon}\sum_j^{NE} \nabla\times\nabla\times\mathbf{\Phi}_j\mathbf{E}_j^{n+1} = \mathbf{E}_i^{n} + \frac{\Delta t}{\varepsilon}\sum_j^{NH}\nabla\times\mathbf{\Phi}_j\mathbf{H}_j^{n} - \frac{\Delta t^2}{4\mu\varepsilon}\sum_j^{NE}\nabla\times\nabla\times\mathbf{\Phi}_j\mathbf{E}_j^{n}. \quad (11)$$

On the other hand, we collect (8) and its cyclic permutations to obtain the magnetic field in its vector form. Substituting (6a) and (6b) into the obtained vector form of the magnetic field and considering the Kronecker's delta property of the vector shape function lead to obtaining the following explicit equation:

$$\mathbf{H}_i^{n+1} = \mathbf{H}_i^{n} - \frac{\Delta t}{2\mu\varepsilon}\left(\sum_j^{NE}\nabla\times\mathbf{\Phi}_j\mathbf{E}_j^{n} + \sum_j^{NE}\nabla\times\mathbf{\Phi}_j\mathbf{E}_j^{n+1}\right). \quad (12)$$

Equations (11) and (12) form the CN formulation of vector meshless method. After solving the implicit formulation of the electric field in (11), the vector of the magnetic field can be obtained explicitly through (12).

III. Numerical Examples

Here to verify the unconditional stability of our proposed CN formulation of vector meshless method, we have considered a two-dimensional (2-D) air-filled rectangular cavity. The length and width of the cavity are both equal to 1.0 cm, and perfectly conducting walls are located at the edges. A point source of Gaussian pulse as the excitation source is located inside the cavity [17]. The spatial domain of the cavity is discretized with a number of nodes, which are scattered regularly in the problem domain and its boundary. The nodal spacing is taken to be 0.5 mm. In order to enforce the perfect electric conductor boundary condition, we set the magnitude of the tangential components of the electric field equal to zero at the nodes that are located at the boundaries using the specific location of each node.

First by simulating the cavity with the conventional vector meshless method, we obtained $\Delta t_{\max}$ as the maximum time-step size, which ensures the stability of the conventional vector meshless method. Then, to investigate the stability of the proposed method in comparison to the conventional vector meshless method, we have considered some larger time-steps than $\Delta t_{\max}$ in simulating the problem with the CN vector meshless methods. Fig. 1 shows that the simulation with the proposed method leads to obtaining stable solutions when the size of time-step is far larger than $\Delta t_{\max}$. In this figure s shows the size of time-step and is equal to $\Delta t/\Delta t_{\max}$.

In order to compare the accuracy of the proposed method with ADI vector meshless method as another unconditionally stable method, we have determined the resonance frequency of the cavity by applying Fourier transform to the transient responses of the proposed method and the ADI vector meshless method. Table I shows a comparison between the accuracy of the simulations through both of the methods in different time-steps. The relative error has been calculated using the analytical resonance frequency of the cavity, which is equal to 44.97 GHz. The results show that choosing a larger time-step leads to a rise in relative errors. On the other hand, the obtained results through

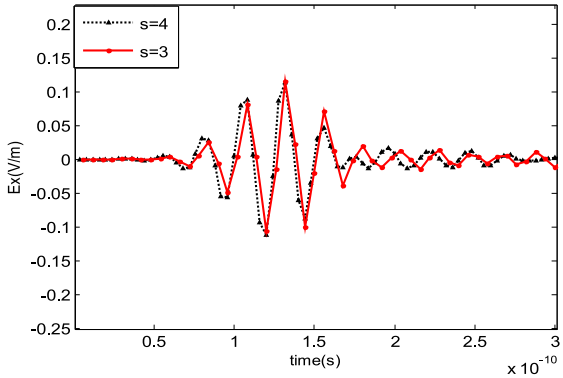

Fig. 1. E_x field recorded at the observation point of the 2-D resonator solved with the proposed CN vector-based meshless method in different time-steps.

TABLE I
Proposed CN Vector Meshless Method and ADI Vector Meshless Method Simulation Results in Different Time-Steps

Method	$\Delta t/\Delta t_{\max}$	Resonance Frequency (GHz)	Relative Error (%)
CN vector meshless	3	44.92	0.11
	4	44.66	0.69
	5	42.52	5.45
ADI vector meshless	3	43.76	2.7
	4	42.52	5.45
	5	42.02	6.6

TABLE II
Computational Cost for the Two Methods

Method	$\Delta t/\Delta t_{\max}$	CPU Time (10^{-1} s)	Memory (Mb)
CN vector meshless	1	34.3	6
	3	23.7	6
	4	20.9	6
ADI vector meshless	1	42.3	6
	3	27.5	6
	4	25	6

the CN vector meshless are more accurate than those of the ADI vector meshless method.

In Table II, we have compared the computational cost of the proposed method in different time-steps with ADI vector meshless method. It can be seen that the CPU time of the CN vector meshless method is less than its ADI counterpart, while memory requirements of both of these methods are similar to each other.

In order to solve implicit equations of the CN and ADI formulations of vector meshless method, we have to compute the inverse of a matrix for each method. The shape parameter of the scalar RBF influences the condition numbers of these matrices [16]. If the condition number is not very large, its inverse can be computed with small numerical errors. In Fig. 2, we have investigated the impact of changing the shape parameter on the condition numbers of the CN and ADI vector meshless methods. According to Fig. 2, the condition number of matrix of the proposed CN vector meshless method is smaller than its ADI counterpart. Therefore, the solution of implicit equation of unconditionally stable vector meshless method based on the CN scheme can be more precise than ADI scheme.

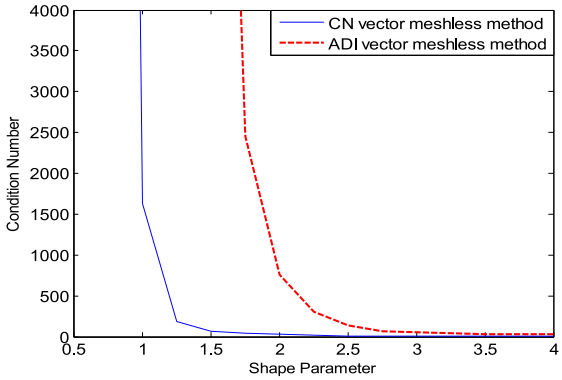

Fig. 2. Condition number of the matrices of the CN and ADI vector meshless methods in different shape parameters (α) of the Gaussian RBF.

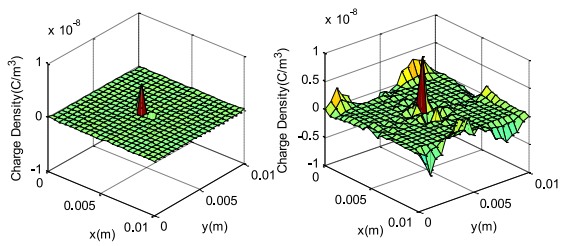

Fig. 3. (a) Charge distribution obtained with the CN vector meshless method and (b) scalar RBF meshless method at $t = 1.5 \times 10^{-10}$ s.

In vector meshless methods that are formulated based on the unconditionally stable algorithms, although choosing a larger shape parameter reduces the condition number of their matrices and leads to more accurately solving the implicit equations, the accuracy of interpolation reduces due to using a large shape parameter. Hence, we should find the smallest shape parameter to improve the accuracy of interpolation and, on the other hand, this shape parameter should be large enough to provide a small condition number for more precisely solving the implicit equations.

In order to investigate the divergence property of our proposed method, we locate a point current source at the center of the mentioned air-filled cavity and obtain the electric charge distribution by the following principle:

$$\rho = \nabla \cdot \varepsilon \mathbf{E} = \frac{\partial \varepsilon E_x}{\partial x} + \frac{\partial \varepsilon E_y}{\partial y}. \tag{13}$$

It is expected to observe a strong charge distribution at the center of the cavity while the electric charge density must be equal to zero in source-free regions. Fig. 3 presents a comparison between the electric charge distribution obtained through the scalar RBF meshless method and the proposed CN vector meshless method. According to Fig. 3, using our proposed method the electric charge density is concentrated at the position of the source while there are no charges elsewhere. However, the scalar RBF meshless method leads to obtaining a large distribution of spurious charges in source-free regions. Therefore, the simulation using the CN vector meshless method can be more accurate than the scalar RBF meshless method due to providing divergence-free solutions in source-free regions. For more details, please refer to our previous publication [10].

IV. Conclusion

In this letter, by incorporating CN scheme into vector meshless method, we have introduced an unconditionally stable divergence-free vector meshless method. The proposed method can decrease the simulation time because of being stable in larger time-steps than the stability limit. However, increasing the size of time-steps is restricted due to the numerical errors. On the other hand, in comparison to ADI vector meshless method, the proposed CN vector meshless method leads to obtaining more precise solutions and is also computationally more efficient.

References

[1] S. J. Lai, B. Z. Wang, and Y. Duan, "Meshless radial basis function method for transient electromagnetic computations," *IEEE Trans. Magn.*, vol. 44, no. 10, pp. 2288–2295, Oct. 2008.

[2] S. Yang, Z. Chen, Y. Yu, and S. Ponomarenko, "A divergence free meshless method based on the vector basis function for transient electromagnetic analysis," *IEEE Trans. Microw. Theory Techn.*, vol. 62, no. 7, pp. 1409–1415, Jul. 2014.

[3] G. Sun and C. W. Trueman, "Unconditionally stable Crank–Nicolson scheme for solving the two-dimensional Maxwell's equations," *Electron. Lett.*, vol. 39, pp. 595–597, Apr. 2003.

[4] G. Sun and C. W. Trueman, "Approximate Crank-Nicolson schemes for the 2-D finite-difference time-domain method for TEz waves," *IEEE Trans. Antennas Propag.*, vol. 52, no. 11, pp. 2963–2972, Nov. 2004.

[5] M. Movahhedi, A. Abdipour, A. Nentcheve, M. Dehghan, and S. Selberherr, "Alternating direction implicit formulation of the finite-element time-domain method," *IEEE Trans. Microw. Theory Techn.*, vol. 55, no. 6, pp. 1322–1331, Jun. 2007.

[6] H. Zhu, C. Gao, and H. Chen, "An unconditionally stable radial point interpolation method based on Crank-Nicolson scheme," *IEEE Antennas Wireless Propag. Lett.*, vol. 16, pp. 393–395, 2017.

[7] Y. Yu and Z. Chen, "Towards the development of an unconditionally stable time-domain meshless numerical method," *IEEE Trans. Microw. Theory Techn.*, vol. 58, no. 3, pp. 578–586, Mar. 2010.

[8] Y. Yu and Z. Chen, "A hybrid ADI-RPIM scheme for efficient meshless modeling," in *Proc. Int. Symp. IEEE MTT-S Microw.*, Baltimore, MD, USA, Jun. 2011.

[9] S. Shams, A. Ghafourzadeh-Yazdi, and M. Movahhedi, "Unconditionally stable vector-based meshless method for transient electromagnetic analysis," in *Proc. 24th Iranian Conf. Electr. Eng.*, Shiraz, Iran, 2016.

[10] S. Shams, A. Ghafoorzadeh-Yazdi, and M. Movahhedi, "Unconditionally stable divergence-free vector-based meshless method for transient electromagnetic analysis," *IEEE Trans. Microw. Theory Techn.*, vol. 65, no. 6, pp. 1929–1938, Jun. 2017.

[11] G. Sun and C. W. Trueman, "An unconditionally-stable FDTD method based on the Crank–Nicolson scheme for solving the three-dimensional Maxwell's equations," *Electron. Lett.*, vol. 40, no. 10, pp. 589–590, May 2004.

[12] Y. Yu and Z. Chen, "A 3-D radial point interpolation method for meshless time-domain modeling," *IEEE Trans. Microw. Theory Techn.*, vol. 57, no. 8, pp. 2015–2020, Aug. 2009.

[13] S. Lowitzsch, "Approximation and interpolation employing divergence-free radial basis functions with applications," Ph.D. dissertation, Dept. Math., Texas A&M Univ., College Station, TX, USA, 2002.

[14] S. Lowitzsch, "Matrix-valued radial basis functions: Stability estimates and applications," *Adv. Comput. Math.*, vol. 23, no. 3, pp. 299–315, Oct. 2005.

[15] S. Lowitzsch, "A density theorem for matrix-valued radial basis functions," *Numer. Algorithms*, vol. 39, no. 1–3, pp. 253–256, Jul. 2005.

[16] T. Kaufmann, C. Engstrom, C. Fumeaux, and R. Vahldieck, "Eigenvalue analysis and longtime stability of resonant structures for the meshless radial point interpolation method in time domain," *IEEE Trans. Microw. Theory Techn.*, vol. 58, no. 12, pp. 3399–3408, Dec. 2010.

[17] H. Razmjoo, M. Movahhedi, and A. Hakimi, "Electromagnetic time domain modeling using an improved meshless method," in *Proc. Int. Symp. IEEE MTT-S Microw. Digest*, 2011, pp. 1–4.